Nonlin. Processes Geophys., 17, 499–512, 2010
www.nonlin-processes-geophys.net/17/499/2010/
doi:10.5194/npg-17-499-2010

Nonlinear Processes in Geophysics

Complex behaviour and predictability of the European dry spell regimes

X. Lana[1], **M. D. Martínez**[2], **C. Serra**[1], **and A. Burgueño**[3]

[1]Departament de Física i Enginyeria Nuclear, Universitat Politècnica de Catalunya, Barcelona, Spain
[2]Departament de Física Aplicada, Universitat Politècnica de Catalunya, Barcelona, Spain
[3]Departament de Meteorologia i Astronomia, Universitat de Barcelona, Barcelona, Spain

Received: 11 May 2009 – Revised: 15 July 2010 – Accepted: 23 August 2010 – Published: 30 September 2010

Abstract. The complex spatial and temporal characteristics of European dry spell lengths, DSL, (sequences of consecutive days with rainfall amount below a certain threshold) and their randomness and predictive instability are analysed from daily pluviometric series recorded at 267 rain gauges along the second half of the 20th century. DSL are obtained by considering four thresholds, R_0, of 0.1, 1.0, 5.0 and 10.0 mm/day. A proper quantification of the complexity, randomness and predictive instability of the different DSL regimes in Europe is achieved on the basis of fractal analyses and dynamic system theory, including the reconstruction theorem. First, the concept of lacunarity is applied to the series of daily rainfall, and the lacunarity curves are well fitted to Cantor and random Cantor sets. Second, the rescaled analysis reveals that randomness, persistence and anti-persistence are present on the European DSL series. Third, the complexity of the physical process governing the DSL series is quantified by the minimum number of nonlinear equations determined by the correlation dimension. And fourth, the loss of memory of the physical process, which is one of the reasons for the complex predictability, is characterized by the values of the Kolmogorov entropy, and the predictive instability is directly associated with positive Lyapunov exponents. In this way, new bases for a better prediction of DSLs in Europe, sometimes leading to drought episodes, are established. Concretely, three predictive strategies are proposed in Sect. 5. It is worth mentioning that the spatial distribution of all fractal parameters does not solely depend on latitude and longitude but also reflects the effects of orography, continental climate or vicinity to the Atlantic and Arctic Oceans and Mediterranean Sea.

Correspondence to: X. Lana
(francisco.javier.lana@upc.edu)

1 Introduction

As in many other fields of Geosciences, fractal concepts are very useful for a better knowledge of the physical laws governing the complex natural processes of the pluviometric regimes and their time predictability. The applicability of these physical laws (differential equations of the atmospheric dynamics) is limited by several factors such as their intrinsic complexity, the necessity of reliable data (empirical initial conditions free of errors) to solve the equations, and the effects of a complex topography. In this paper, the fractal analysis is constrained to a particular aspect of a pluviometric regime: the dry spell lengths, DSL, which can be defined as the number of consecutive days with rain amounts lowering a certain threshold R_0 (mm/day).

The fractal nature of rainfall processes is an accepted fact, confirmed by numerous studies along the last decades. It can be cited Lovejoy and Mandelbrot (1985), Rodríguez-Iturbe et al. (1989), Olsson et al. (1993), Hubert et al. (1993), Tessier et al. (1996), Harris et al. (1996), Veneziano et al. (1996), Svensson et al. (1996), Lima and Grassman (1999), Mazzarella (1999), Mazzarella and Tranfaglia (2000), Sivakumar (2001a, b), Sivakumar et al. (2001), Salas et al. (2005) and Martínez et al. (2007a), among many others. Multifractality, chaotic behaviour, time persistence and predictability have been concepts considered by these authors and many variables closely related to rainfall regimes have been analysed. Rain intensity, annual amounts, precipitation linked to convective storms, rain gauge network design and episodes of dry spell lengths are some illustrative examples.

Notable efforts have been devoted along many years to analyse dry spells from a statistical point of view, quantifying for instance return periods for severe drought episodes, and several drought indices have been developed and proposed in Hydrology and Climatology for a better quantification of the drought phenomena. Nevertheless, analyses of predictability

Published by Copernicus Publications on behalf of the European Geosciences Union and the American Geophysical Union.

of the DSL series, necessary for a better prediction of drought periods, are not so common in the scientific literature. These analyses of predictability should include estimation of possible random components, complexity of the physical mechanisms generating the DSL episodes, predictive instability of the equations governing the process, and qualification of chaotic behaviour.

The analysis developed in this study is based on the nonlinear character of the DSL series and it consists of four steps involving lacunarity, rescaled analysis, the reconstruction theorem and predictive instability. The main objective is to analyse spatial and temporal fractal patterns of the dry spell regime in Europe, which cannot be described by means of statistical tools, as those used, for instance, by Lana et al. (2004, 2006), Burgueño et al. (2005), Martínez et al. (2007b), who made use of statistical distributions, return periods and spectral analyses for studying the dry spell behaviour of NE Spain and the Iberian Peninsula.

A similar analysis was performed by Martinez et al. (2007a) for DSL series on the Iberian Peninsula. The present paper should not be considered as a simple extension to a broader area. First, an interpretation of the lacunarity in terms of Cantor and random Cantor sets is for the first time successfully attempted now. Second, results concerning rescaled analysis and predictive instability (Lyapunov exponents) for the Iberian Peninsula can be compared now with those obtained for the rest of Europe. Third, the analyses based on the reconstruction theorem, not applied by Martínez et al. (2007a), are now developed for the European database. In addition, the concept of Kaplan-York dimension is used also for the first time to characterise other aspects of the predictive instability for European DSL series. In this way, common patterns and outstanding differences on the dry spell regimes throughout Europe would be manifested.

The contents of the paper are arranged as follows. Collected database and methodology are introduced in Sects. 2 and 3, respectively. Section 4 is devoted to introduce the main concepts, basic formulations and results concerning lacunarity, rescaled analysis and reconstruction theorem (complexity and predictive instability). The most relevant results and conclusions regarding the fractal analysis of DSL regimes in Europe are summarised in Sect. 5.

2 Databases

The database consists of 267 time series of daily rainfall records corresponding to European rain gauges. These time series were previously compiled, and their quality and homogeneity checked, by Klein Tank et al. (2002) and Wijngaard et al. (2003). These data series are available at http://eca.knmi.nl. Some of the Spanish data come from the *Agencia Estatal de Meteorología* (Spanish Ministry of Environment) and similar homogeneity and quality controls were applied (Lana et al., 2006). Figure 1a depicts the spatial distribution of these rain gauges. It can be observed that

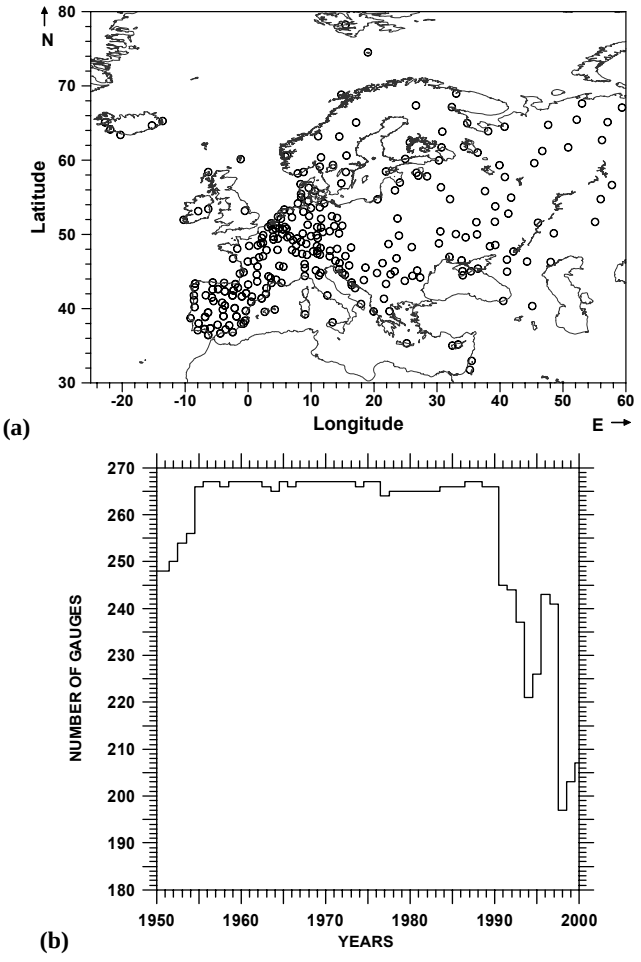

Fig. 1. (a) Spatial distribution of the 267 rain gauges in Europe. **(b)** Number of available records per year along the recording period.

for longitudes east of 15° E and latitudes north of 55° N the density of rain gauges decreases remarkably. For this reason, the discussion and interpretation of the fractal parameters will be especially restricted to areas within these limits in latitude and longitude. Figure 1b shows the evolution of the number of available records by year. The lack of data is almost null for the 1955–1990 recording period. At the beginning (1951–1955) and at the end (1990–2000) of the recording period, the number of available records diminishes, especially from 1998 to 2000. Given that all the fractal analyses require long enough series, not necessarily with common starting and ending years, slightly different periods with good recording continuity are selected for every station within years 1950–2000. Dry spells including periods with isolated lack of records (at least a day with missing data) have been discarded from the analysis because those DSL could be fictitious. The removal of these uncertain DSLs from the time series could bias the values of the fractal parameters. However, this undesirable effect would be only remarkable if there was a massive lack of data for specific rain gauges, which is not the case for our database.

3 Methodology

The concept of lacunarity introduced by Mandelbrot (1982), which can be interpreted as a measure of clustering of gap sizes in data series, is applied to the series of daily rainfall. Given that the introduction of thresholds is needed for defining "gaps" in these series, lacunarity curves are computed for four thresholds, R_0, of 0.1, 1.0, 5.0 and 10.0 mm/day. These same levels are considered to derive four different DSL series for every rain gauge. Lacunarities are then computed by using moving windows of increasing length, r, from 1 to 100 days, thus covering different time scales as days, weeks, months and seasons. As shown later, every lacunarity curve is well described for every rain gauge by two power laws with exponents and changing points depending on R_0. Additionally, in agreement with the basic lacunarity concept (a cluster measure) and the intrinsic behaviour of DSL (lengths increasing with the threshold), it is convenient to check that lacunarity values increase systematically with R_0. In addition, the best fit of empirical to synthetic lacunarities generated by Cantor or random Cantor sets is determined by comparing the corresponding misfits. It is worth mentioning that empirical curves reproduced by Cantor sets could represent pluviometric regimes governed by relevant deterministic mechanisms, without excluding certain random components. On the contrary, lacunarities governed by random Cantor sets should be related to pluviometric regimes with very relevant random components. A deterministic example could be the Devil's staircase model (Fedder, 1988), which is defined as the cumulative Cantor set. Then, for instance, a Cantor set can reproduce the sediment deposition rate paradox, and a Devil's staircase a stratigraphic thickness sequence (Korvin, 1992). An example of random behaviour is found in the analysis of the monthly North Atlantic Oscillation, NAO, index, where lacunarity curves are well reproduced by a random Cantor set (Martínez et al., 2010).

Additional information regarding the deterministic or random character of a pluviometric regime could be obtained through the rescaled analysis (Fedder, 1988; Korvin, 1992; Turcotte, 1997), which is applied to the DSL series derived for the different levels R_0. The interpretation of the Hurst exponent, H, provides additional details which reinforce the deterministic or random character of the series analysed. It should be remembered that H close to 0.5 is a clear sign of randomness. On the contrary, H well above 0.5 suggests persistence (time trends on previous DSL series contribute to DSL prediction) and H well below 0.5 suggests anti-persistence (an average of all previous DSL values contributes to DSL prediction). Then, Hurst exponents contribute to a better knowledge of the time behaviour of the dry spell lengths, a very relevant question for assessing hazards concerning water resources and supplies.

Beside lacunarity and rescaled analyses, which quantify gap clustering and randomness versus predictability respectively, an additional insight into the characterization of the dynamical system governing the dry spell time sequence and its predictability is achieved by means of the reconstruction theorem (Grassberger and Procaccia, 1983a; Diks, 1999). Three main parameters are derived from this reconstruction process. First, the correlation dimension, μ^*, can be estimated from the analysis of the correlation integral curves (Grassberger and Procaccia, 1983a). This parameter represents the minimum number of nonlinear equations needed for describing the physical mechanism. Second, the Kolmogorov entropy, κ, is also determined from the same correlation curves (Grassberger and Procaccia, 1983b; Cohen and Procaccia, 1983). It represents the loss of memory of the physical process and it could be taken to some extent as a reference for the number of consecutive dry spell lengths to be considered in autoregressive predictive processes. The reconstruction process of the DSL series, for every level R_0 and rain gauge, is repeated by successively increasing dimension m. This process can be shortened and automated under some conditions developed in the present manuscript. A fast automated method for computing κ is proposed and μ^* is assumed to be the asymptotic value of the slope of the correlation integral curve for a high enough reconstruction dimension m of the DSL series. And third, the Lyapunov exponents (Turcotte, 1997) for a reconstruction dimension m, which quantify the degree of predictive instability of the DSL series, are computed by following an algorithm proposed by Eckmann et al. (1986) and Stoop and Meier (1988). Additionally, the Kaplan-Yorke dimension (Kaplan and Yorke, 1979; Grassberger et al., 1991; Diks, 1999) is evaluated taking into account all Lyapunov exponents for every DSL series. Then, the fractal dimension of the strange attractor representing the dynamical system governing DSL can be quantified.

4 Formulation and results

4.1 Lacunarity

The lacunarity is a way of quantifying the distribution of gap sizes within a set of data (Mandelbrot, 1982). It also represents the measure of the failure of a fractal to be transitionally invariant and plays a relevant role in the study of critical phenomena. Additionally, several fractal sets with the same fractal dimension can be distinguished by their lacunarities, due to their different gap distribution. Large lacunarities imply large gaps and clumping of points, whereas small lacunarities suggest a rather uniform distribution of small gaps. Several illustrative examples can be found in Turcotte (1997), where quite uniform and clumped distributions are related to small and high lacunarities, respectively. Other examples of lacunarity are those corresponding to series generated by Cantor and random Cantor sets.

An alternative to the analysis in terms of lacunarity is given by the concept of the cluster dimension D (Korvin, 1992). Some examples in Climatology and Seismology can

be found in Mazzarella (1999) and Lana et al. (2005), respectively. Very briefly, referring to the daily rainfall series, the more isolated the clusters of rainy days, the smaller the value of D. Thus, small values of D should be related to high values of lacunarity L. On the contrary, high values of D should represent quite uniformly distributed consecutive rainy days, only separated by short gaps, which would correspond to low values of L.

At the present application, lacunarity represents a measure of the distribution of segments, defined as the number of consecutive days with rain amounts equalling or exceeding some threshold values R_0, and gaps, introduced as the number of consecutive days with rain amounts below R_0. The probability of detecting s segments within a moving window of length r (in days) is given by

$$p(s,r) = n(s,r)/N(r) \tag{1}$$

where $N(r)$ is the total number of possible windows of length r, that is $N(r) = \ell - r + 1$, with ℓ the whole number of recording days. $n(s,r)$ is the number of moving windows of length r containing s segments. Finally, the lacunarity, as a function of the segment length, r, is defined as

$$L(r) = \frac{M_2(r)}{[M_1(r)]^2} \tag{2}$$

with

$$M_1(r) = \sum_{s=1}^{r} s \cdot p(s,r)\,; \quad M_2(r) = \sum_{s=1}^{r} s^2 \cdot p(s,r) \tag{3}$$

the first and second order moments of r.

The evolution of the lacunarity for the 267 series is analysed by means of moving windows of length r ranging from 1 to 100 days, which is equivalent to consider short (daily), medium (monthly) and long (seasonal) scales.

Figure 2 depicts an example of the evolution of $L(r)$ at a particular rain gauge for the four levels R_0. As expected from the concept of lacunarity and Eqs. (1)–(3), $L(r)$ tends to 1.0 for r tending to ∞ and the lacunarity increases systematically with the threshold R_0. Moreover, the evolution of $L(r)$ with r can be analytically described by two power laws for every R_0

$$L(r) = \alpha_1 \cdot r^{\beta_1}\,; \quad r = 1, \ldots, r_c \tag{4}$$

$$L(r) = \alpha_2 \cdot r^{\beta_2}\,; \quad r = r_c, \ldots, \ell \tag{5}$$

with parameters (α_1, β_1) changing to (α_2, β_2) for a critical window length r_c. Parameters α_1, β_1, α_2 and β_2 of the power laws (4a, b) are determined by linear regression on a log-log scale. The critical value r_c is the value leading to the best square regression coefficient for segments within intervals $[1 - r_c]$ and $[r_c - \ell]$. A systematic analysis of the 267 time series for the four threshold levels permits to ascertain that all lacunarity curves fulfil Eqs. (4) and (5). Given that the most relevant changes in lacunarity are always detected before the critical value r_c, Fig. 3 represents the geographical distribution of parameters α_1 and β_2 and critical lengths r_c, for the four thresholds R_0.

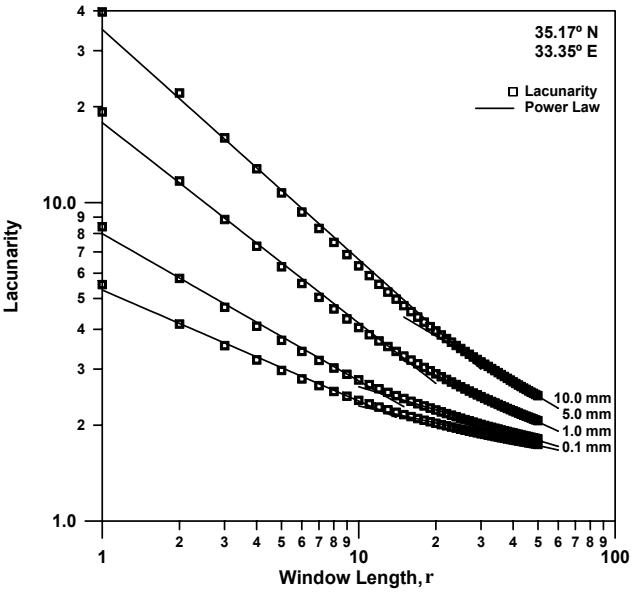

Fig. 2. An example of lacunarity curves for a daily rainfall series and the four thresholds (0.1, 1.0, 5.0 and 10.0 mm/day).

Maps of α_1 (Fig. 3a) represent the lacunarity at daily scale, as $L(1)$ is equal to α_1. For the first three levels R_0, it can be observed a northwest-southeast gradient of α_1 in the Iberian Peninsula and Eastern Mediterranean. The highest lacunarities are reached in the south of the Iberian Peninsula. The rest of Europe, except the Eastern Mediterranean, is characterised by an almost constant value of α_1. Some signs suggesting a more complex spatial distribution for 5.0 mm/day are confirmed in the 10.0 mm/day map, with outstanding lacunarities in Eastern Europe and latitudes north of 60° N. High lacunarities are still observed in the Southern Iberian Peninsula for 10.0 mm/day map. Maps of parameter β_1 (Fig. 3b) describe the spatial distribution of the power decay of lacunarity when increasing moving window length r (days). It is relevant that the fastest decay of lacunarity is reached for some areas faced to the Atlantic Ocean (West of the Iberian Peninsula and Scandinavia for instance) and close to the Alps, whatever the level R_0.

Maps of Fig. 3c show the geographical distribution of the critical values of r_c. Differences are very remarkable, especially for the first three levels of R_0, with the longest r_c, related to notable reductions of $L(r)$, detected in the Iberian Peninsula. Notably lower values are found for North, Central and Eastern Europe. Once again, the distribution of r_c for 10.0 mm/day is more complex than for the rest of thresholds. Strong gradients in the Iberian Peninsula and a remarkable increase of r_c for many other areas of Europe are

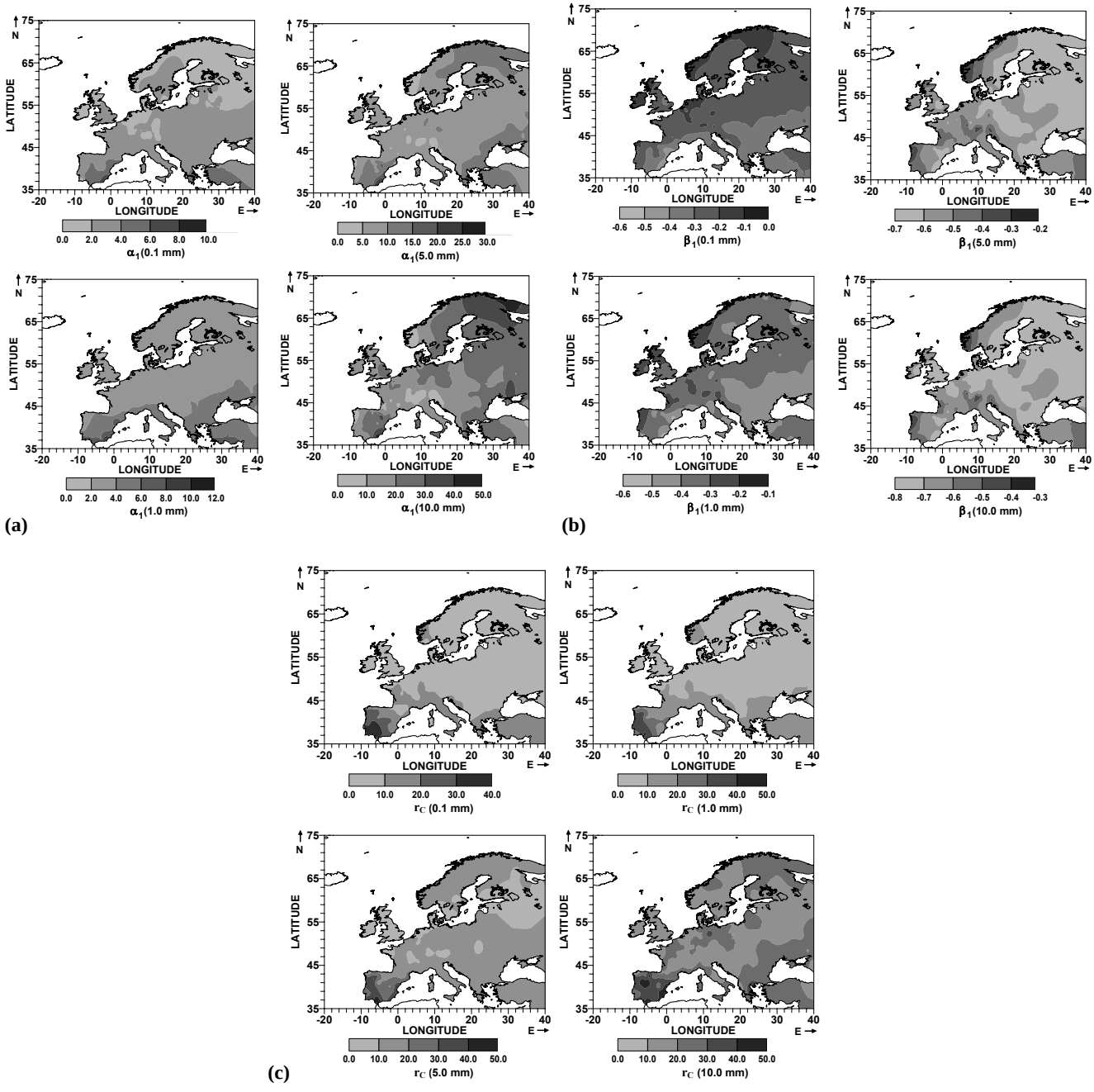

Fig. 3. **(a)** Spatial distribution of parameter α_1 in the power law relating lacunarities and moving window lengths, for 0.1, 1.0, 5.0 and 10 mm/day. **(b)** The same distribution for parameter β_1. **(c)** Spatial distribution of the critical value, r_c, for the same thresholds.

observed, which could be reasonably expected taking into account that gap sizes in rainfall series tend to increase with the threshold level R_0. In short, areas with long-lasting rainfall deficits (high values of r_c) would be characterised by low absolute values of β_1. On the contrary, in areas with short rainfall deficits (low values of r_c), absolute values of β_1 would be high, and the lacunarity relevantly decreases in a limited range of days. It should be emphasised that in many places of Europe the decrease of the lacunarity becomes quite irrelevant for r_c longer than 10–20 days, especially for 0.1, 1.0 and 5.0 mm/day, in contrast with other areas where 40–50 days are necessary.

Additional valuable information can be obtained from lacunarity curves if they can be reproduced by series generated from Cantor or random Cantor sets. The fractal dimension of the Cantor set is equal to $\log 2/\log[(1-G)/2]$ (Korvin, 1992), given that for each iteration of the Cantor set

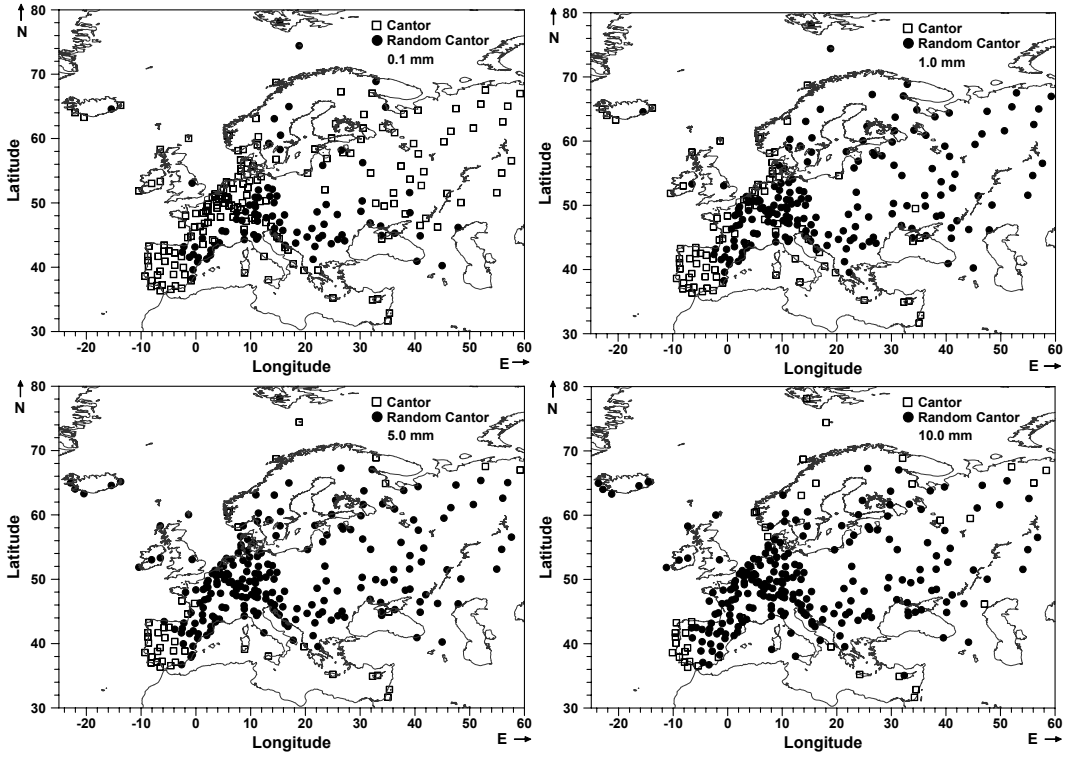

Fig. 4. Spatial distribution of sites where lacunarity curves are best fitted to Cantor (open squares) or random Cantor (solid circles) sets.

generation an element is fragmented into two new pieces and a gap of relative size G. If empirical lacunarity curves are well fitted to random Cantor series, there are clear signs of randomness governing the daily rainfall process, especially if this fit is confirmed for all the R_0 values. Conversely, if empirical lacunarity curves are best fitted to a Cantor set, it can be assumed that a deterministic behaviour is more relevant in the rainfall process that a possible background randomness. This kind of analysis, discriminating between pure randomness and pure deterministic behaviours, has been recently applied to monthly series of the North Atlantic Oscillation (NAO) index (Martínez et al., 2010).

Figure 4 shows the spatial distribution of sites where lacunarity curves are best fitted to random Cantor or Cantor sets. It is observed that a pure single model (either random or deterministic) for all the rainfall series would be an excessively simple description. First, the number of lacunarity curves best fitted to a random Cantor model increases with R_0. Second, although for 10.0 mm/day many lacunarity curves, mostly corresponding to the Atlantic coast of the Iberian Peninsula and to high latitudes, are best fitted to a random Cantor set, a non negligible number of empirical lacunarities are not well enough fitted to any of the two models. Table 1 summarises the results of the fits obtained for the different levels R_0. It is observed that the expected value of the relative gap size, G, generating the best fit to deterministic/random Cantor lacunarities tends to increase with R_0, in agreement with the increase of empirical lacunarities with R_0. Whereas for 0.1, 1.0 and 5.0 mm/day the ratio of lacunarity curves best fitted to a random Cantor set increases, with only a small ratio (null for 0.1 and 1.0 mm/day) of average misfits between empirical and synthetic lacunarities exceeding 0.5, this ratio increases up to 32% for 10.0 mm/day. In consequence, a single model reproducing the lacunarity curves of the different pluviometric regimes of Europe cannot be established. First, the random Cantor set tends to be dominant, but is never the single best model. On the other hand, although the ratio of local pluviometric regimes simulated by this model tends to increase with R_0, a notable number of rainfall series cannot be fitted either to the random or deterministic Cantor model.

Table 1. Average relative gap size, $< G >$, and standard deviation, SD(G), of the lacunarity curves for 267 rainfall daily series and four thresholds R_0. C and RC are the percentage of lacunarity curves fitted to Cantor and random Cantor sets, respectively. MF designs the ratio of empirical lacunarity curves not well enough fitted to any of the two models.

R_0 (mm/day)	$< G >$	SD(G)	C (%)	RC (%)	MF (%)
0.1	0.10	0.05	59.2	40.8	0.0
1.0	0.16	0.04	31.7	68.3	0.0
5.0	0.25	0.04	15.8	84.2	4.5
10.0	0.38	0.08	14.7	85.3	32.1

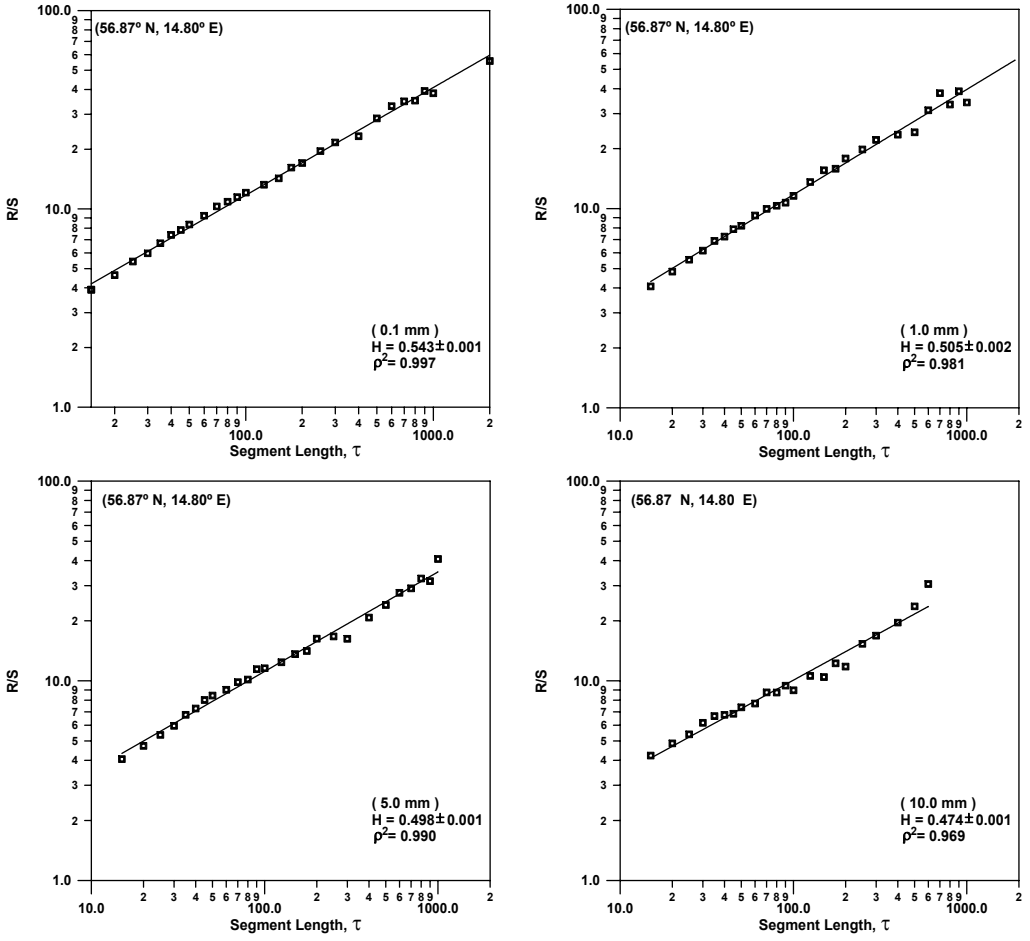

Fig. 5. An example of rescaled analysis for the DSL series and the four thresholds (0.1, 1.0, 5.0 and 10.0 mm/day).

4.2 Rescaled analysis

The rescaled analysis, and more specifically the Hurst exponent (Fedder, 1988; Goltz, 1997), provides us with criteria to qualify the predictability of a complex dynamic system such as the dry spell regime. Applications to a variety of fields in Geology and Geophysics are shown by Korvin (1992) and Turcotte (1997). Some applications in Climatology and more specifically to rainfall regimes can be found in Oñate (1997), Miranda and Andrade (1999, 2001), Whiting et al. (2003), Miranda et al. (2004) and Martínez et al. (2007a), among others.

The predictability of the DSL series is quantified by interpreting the meaning of the Hurst exponent H. For every DSL series, mean values and cumulative differences are computed for subsets of DSL series with different number of elements τ. After that, maximum range, $R(\tau)$, of the integrated signal and standard deviation, $s(\tau)$, for the subsets are computed. If the fractal behaviour exists, the relationship

$$R(\tau)/S(\tau) = a \cdot \tau^{H} \tag{6}$$

is accomplished. As mentioned in Sect. 3, the value of H and its uncertainty are useful tools to quantify the randomness, persistence or anti-persistence of the physical process governing the sequence of dry spells. The reliability of the estimated values of H is based on three constraints. First, a low uncertainty on H; second, an acceptable square regression coefficient for the representation of $\log\{R/S\}$ in terms of $\log(\tau)$; third, the linear evolution of the log-log plot should cover at least two magnitude orders of τ.

Figure 5 shows an example of rescaled analysis for a rain gauge and the four levels R_0. It can be observed that the squared regression coefficient exceeds 0.96 in all cases, the uncertainty on H affects the second decimal digit and the requirement of a minimum of two magnitude orders for τ is also accomplished. Values of τ less than 10 have not been considered to avoid computational artefacts. This is an example where the randomness of the physical process governing dry spells would be relevant, as all Hurst exponents are very close to 0.5.

The same procedure for obtaining the Hurst exponent H shown in Fig. 5 is repeated for the other 266 series and the four levels R_0. Figure 6 shows the spatial distribution of H

throughout Europe for the four thresholds. The thick contour line ($H = 0.5$) delimits areas of persistence and anti-persistence. For 0.1 mm/day, some sites at low latitudes are characterised by anti-persistence, whereas H exceeds 0.5 for the rest of Europe. A quite similar pattern is obtained for 1.0 mm/day, with a nucleus of anti-persistence in the Scandinavian Peninsula. The spatial distribution is much more complex for the other two levels. Even though the values of H keep within the same range, a simple geographical delimitation of areas of persistence and anti-persistence is not evident. Then, Fig. 6 suggests that the same local rainfall regime frequently generates DSL series with predictive characteristics varying from persistence to anti-persistence depending on the threshold R_0, as for example, in some areas of Scandinavian Peninsula. This is a sign of complexity of the rainfall regime, and particularly, of the DSL series. This feature is to be confirmed by the reconstruction theorem and related parameters quantifying complexity and predictive instability.

4.3 Reconstruction theorem

The reconstruction theorem (Takens, 1981; Grassberger and Procaccia, 1983a, b) permits a useful analysis of the complexity and predictive instability of the rainfall regime and, in particular, of the DSL series. The space of the dynamical system governing the dry spells is reconstructed by generating a set $\{z_j\}$ of m-dimensional vectors

$$z_j = \{x_j, x_{j+1}, \ldots x_{j+m-1}\} \quad j = 1, \ldots, n-m+1 \tag{7}$$

being x_j the elements (lengths given in days) of the DSL series for a given R_0 and m the dimension of the reconstructed space. From the set of vector generated by Eq. (6) the correlation function

$$C(r) = \lim_{N\to\infty} \frac{1}{N^2} \sum_{i,j=1}^{N} H\{r - |Z_i - Z_j|\} \tag{8}$$

is straightforward to compute, where r are distances in the m-dimensional space and $H\{\cdot\}$ is the Heaviside function. According to Diks (1999), $C(r)$ behaves as

$$C(r) = A_m r^{\mu(m)} e^{-m\kappa} \tag{9}$$

$\mu(m)$ being the correlation dimension, A_m the correlation amplitude and κ the Kolmogorov entropy. It should be remembered that for a high enough dimension m, usually designed as embedding dimension, d_E, $\mu^* = \mu(d_E)$ represents the minimum number of nonlinear equations required to describe the physical system governing the DSL series, and κ the loss of memory of this system with time. Consequently, both parameters represent an insight into the complexity and predictability of DSL. For instance, κ could help us to select the number of consecutive DSL elements to be considered in an autoregressive process.

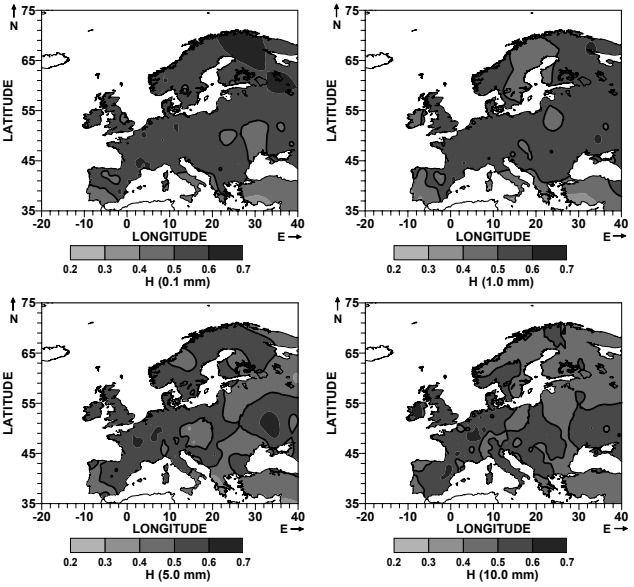

Fig. 6. Spatial distribution of the Hurst exponent for the four thresholds (0.1, 1.0, 5.0 and 10.0 mm/day).

A reiterative search of parameters μ^* and κ for the 267 daily rainfall records and the four thresholds R_0 would be very tedious and time spending. Then, an automated procedure is proposed. If logarithms are taken in Eq. (8)

$$\log\{C(r)\} = \log\{A_m\} + \mu(m)\log(r) - m\kappa \tag{10}$$

the slope of the log-log representation is the correlation dimension, $\mu(m)$, for the m-dimensional space. The correlation curves behave in different ways for three ranges of r. In the first range of r, a quite irregular evolution attributable to the lacunarity and an average slope, notably less than that estimated for the next range of r, are observed. In the second range, an almost perfect linear evolution of $\log\{C(r)\}$ with $\log(r)$ permits to compute $\mu(m)$, which will be the highest slope of the three ranges. For the last range, the correlation function saturates to 1.0 and its average slope is again notably smaller than $\mu(m)$. Consequently, the largest quotient for finite differences of $\log\{C(r)\}$ and $\log(r)$ for moving windows along the correlation curves has to be a good approach of $\mu(m)$. Then, if the correlation curves are calculated for a high dimension m, a stationary value of the correlation dimension, μ^*, is reasonably determined.

Another aspect is the estimation of the Kolmogorov entropy, κ. Coming back to Eq. (9), the slope of the evolution of

$$\alpha(m) = \log\{A_m\} - m\kappa \tag{11}$$

permits an accurate estimation of κ, provided that Eq. (10) is used for a high enough values of dimension m, which is equivalent to assume that $\log\{A_{m+1}/A_m\}$ tends to zero.

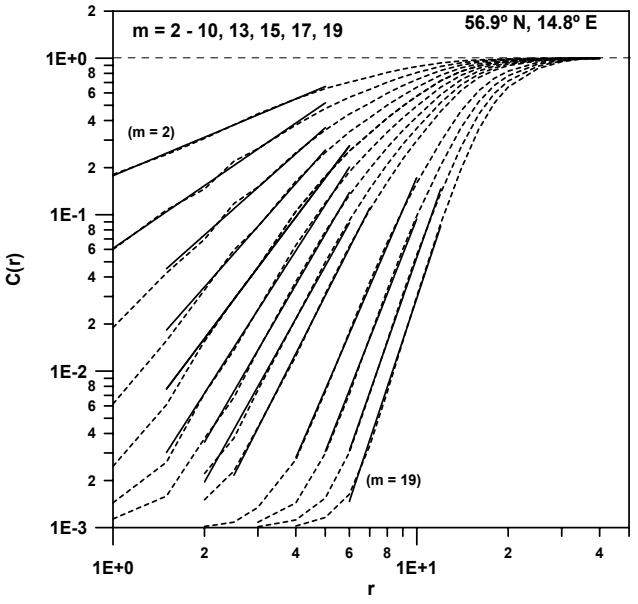

Fig. 7. An example of the correlation function (dashed lines) of a DSL series and linear evolution on a log-log scale (solid line) for m ranging from 2 to 19.

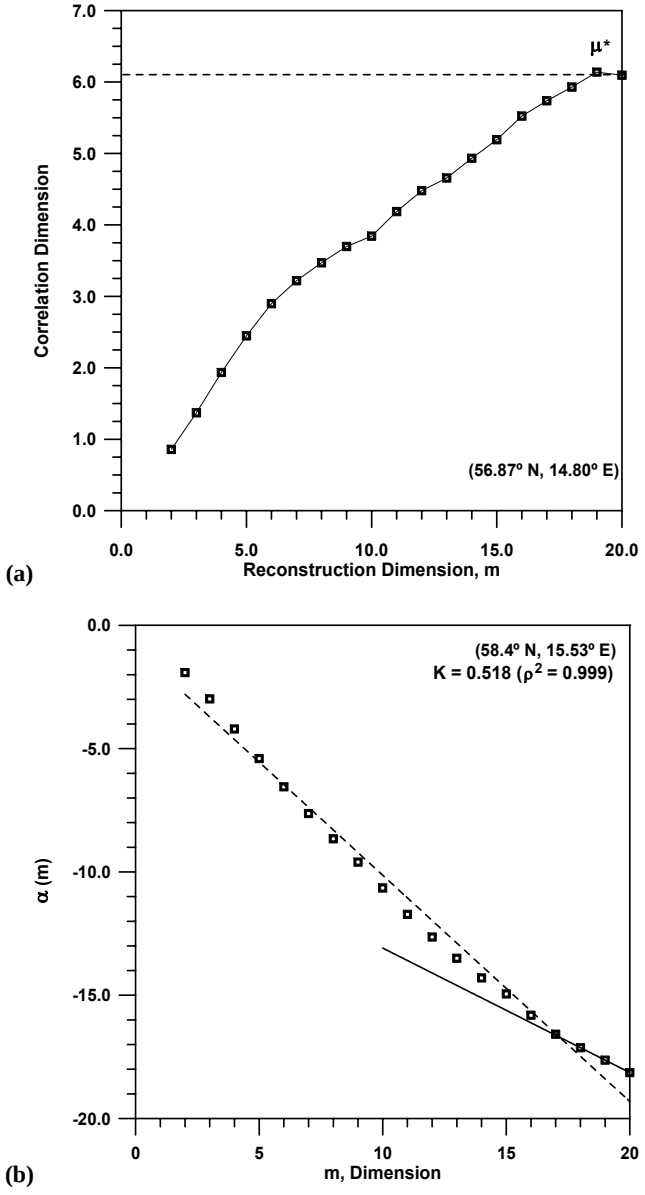

Fig. 8. (a) An example of the evolution of the correlation dimension, μ(m) towards a stationary value, μ^*. **(b)** An example of the right (solid line) and wrong (dashed line) computation of the Kolmogorov entropy.

An example of the assumed behaviour for the $C(r)$ curves of DSL is shown in Fig. 7. The effects of lacunarity are detectable from a dimension m equal to 4 or 5 and saturation to 1.0 is always present, whatever the dimension m. At the same time, the largest slopes, $\mu(m)$, indicated by solid lines, tend asymptotically towards a constant value, μ^*.

Figure 8 depicts an example of the evolution of the correlation dimension and the determination of the Kolmogorov entropy. Remembering the meaning of the correlation dimension (Diks, 1999), it would be necessary at least six nonlinear equations to describe the physical process generating the DSL series. An attempt to quantify more accurately μ^* by exploring reconstruction dimensions m higher than 20 would not be advisable. Three issues need to be discussed. First, the constraint $d_E > 2\mu^* + 1$ for a right quantification of μ^* (Martínez et al., 2010) is still fulfilled, taking into account that the highest exploring dimension is 20 and μ^* is very close to 6.0. Second, as can be observed in the example of Fig. 7, the range of r for which there is a linear relationship between $\log\{C(r)\}$ and $\log(r)$ diminishes with m due to the above mentioned effects of lacunarity and saturation. In consequence, additional estimations of μ could not be extremely accurate. Third, as μ^* is only a lower bound to the required number of nonlinear equations, and considering the evolution of μ for high values of m, a substantial change on μ^* would be unlikely. Finally, some fluctuations in the evolution of μ towards μ^* would be attributable to errors on the slope of the linear relationship between $\log\{C(r)\}$ and $\log(r)$. These errors could be attributable to missing DSLs or departures of $C(r)$ from the power law given by Eq. (8). Remembering how lack of data is managed (Sect. 2), it should be accepted that discarded dry spells might be a cause for these fluctuations.

With respect to the estimation of the Kolmogorov entropy, it is relevant to observe that whereas entropy close to 0.5 is obtained by considering m ranging from 16 to 20, a linear fit for the whole range of m (from 2 to 20) would lead to a wrong determination of κ, close to 0.9. For a right computation, A_m must be very close to A_{m+1}, and the linear fit be almost perfect. On the contrary, considering the whole range of m, the

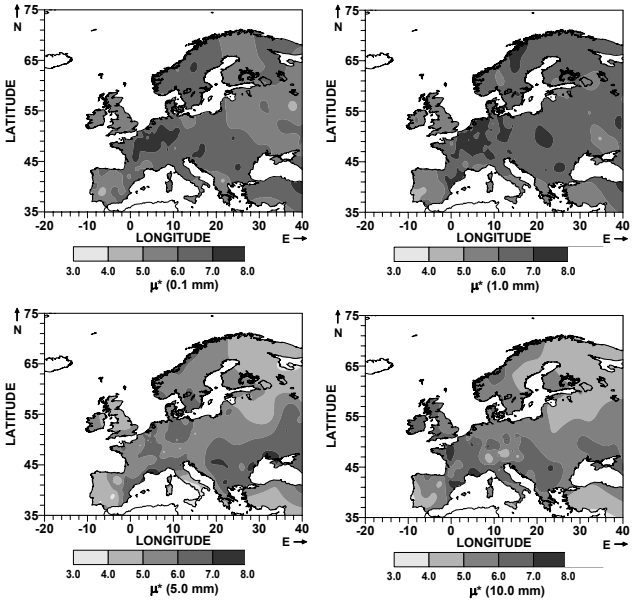

Fig. 9. Spatial distribution of the asymptotic values of the correlation dimension for thresholds of 0.1, 1.0, 5.0 and 10.0 mm/day.

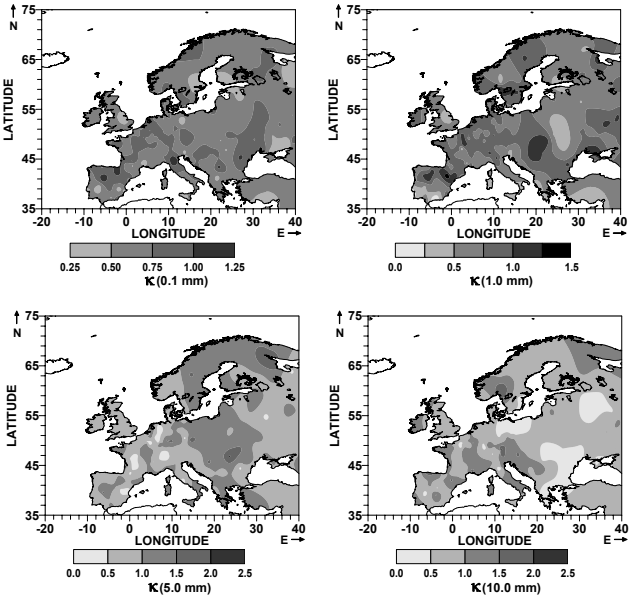

Fig. 10. Spatial distribution of the Kolmogorov entropy for thresholds of 0.1, 1.0, 5.0 and 10.0 mm/day.

linear fit is deceptive and the Kolmogorov entropy is overvalued. An additional issue to be considered is the high dimension m needed to obtain asymptotic values of the correlation dimension and a right estimation of κ. This fact is common to all series and levels R_0. This necessity for a high reconstruction dimension also manifests the complexity of the DSL predictive processes. If the right reconstruction of DSL series was achieved with low dimensions, a dry spell episode would solely depend on a few previous episodes and, possibly, a quite simple autoregressive process could be a good predictive tool. Nevertheless, the real physical process governing DSL series (differential equations of the atmospheric dynamics and effects of the topography, vicinity to oceans, etc) is much more complex. Even higher complexities in the atmosphere-ocean coupled dynamics have been found in the analysis of the NAO index (Martínez et al., 2010).

Figure 9 depicts the spatial distribution of μ^* for thresholds of 0.1, 1.0, 5.0 and 10.0 mm/day. According to Ruelle (1990), the stationary value of the correlation dimension accomplishes $\mu^* < 2\log_e(M)$, being M the number of DSL elements for a series. The values of μ^* for all thresholds R_0 vary within a wide range, from 3 to 8. Their spatial patterns also change with the threshold. In consequence, for every rain gauge, the required minimum number of nonlinear equations changes with R_0. Figure 10 shows that a similar situation is detected for the entropy κ. Besides the range of κ increases with R_0, spatial patterns change depending on the threshold. Once again, additional complexities appear because the loss of memory of the physical system governing DSL depends on the level R_0 and the geographical location of rain gauges. Remembering shortcomings affecting the estimation of μ^* and κ, it is obvious that an automated selection of these two parameters is not convenient and a one-by-one revision for every DSL series is advisable.

4.4 Predictive instability

Associated with the reconstruction theorem and reconstructed vectors, the predictive instability is conceptually defined as the effect of an inaccurate starting state z_0 on the uncertainty on the state z_j, after j-steps of the dynamical system. The validation of this effect could be addressed either to the computation of the largest positive Lyapunov exponent, $\lambda_{\max}$ (the main generator of predictive instability), or the evaluation of the m Lyapunov exponents $\{\lambda_{\max} = \lambda_1 > \lambda_2 > \ldots > \lambda_m\}$. With this second option, Kaplan-Yorke dimensions, D_{KY}, are then determined from the Lyapunov exponents. If the sum of all the Lyapunov exponents is negative, the Kaplan-Yorke dimension is expressed as

$$D_{\mathrm{KY}} = \ell_0 + \frac{1}{\left|\lambda_{\ell_0+1}\right|}\sum_{j=1}^{\ell_0}\lambda_j \qquad (12)$$

being ℓ_0 the largest integer for which $\lambda_1+\lambda_2+\ldots+\lambda_{\ell_0} > 0$. The different states of the reconstructed vectors in the m-dimensional space would generate strange attractors if they could be defined as bounded sets of aperiodic trajectories asymptotically stables and sensitive to initial conditions. The fractal dimension of these strange attractors would be then quantified by the Kaplan-Yorke (or Lyapunov) dimension, D_{KY}.

Table 2. Minimum, maximum and expected values and standard deviations of the sum of all Lyapunov exponents, S_T, and the Kaplan-Yorke, D_{KY}, dimension. Range and expected values of the number, N_P, of positive Lyapunov exponents are also included.

	S_T				N_P		D_{KY}			
R_0 (mm/day)	Min	Max	$< S_T >$	$\sigma(S_T)$	$< N_P >$	Range	Min	Max	$< S_T >$	$\sigma(S_T)$
0.1	–0.99	–0.60	–0.78	0.07	6.7	5–8	12.61	14.08	13.45	0.20
1.0	–0.92	–0.56	–0.79	0.06	6.8	6–7	12.87	14.08	13.42	0.20
5.0	–0.96	–0.49	–0.79	0.07	6.6	5–7	12.89	14.11	13.38	0.21
10.0	–1.21	–0.37	–0.84	0.10	6.6	5–7	10.78	14.40	13.20	0.41

Wolf et al. (1985) proposed an algorithm to compute non-negative Lyapunov exponents, responsible for predictive instability. A more sophisticated computational algorithm (Eckmann et al., 1986; Stoop and Meier, 1988) permits to obtain all the Lyapunov exponents for a reconstruction space of dimension m. The step-by-step detailed procedure of this algorithm can be found in Martínez et al. (2007a). It has to be pointed out that it must be applied for many dimensions m with the aim of obtaining a set of m stationary Lyapunov exponents. As verified by Martínez et al. (2010), it is usual that these stationary values are achieved at values of m less than those corresponding to the embedding dimension, d_E, determined in Sect. 4.3.

Figure 11 summarises the spatial distribution of the first positive Lyapunov exponent, which is the main responsible of predictive instability. As for the previous fractal parameters, the spatial patterns are relatively complex because they change with R_0. For 0.1 and 1.0 mm/day, the dominant value for λ_1 is within a narrow range of 0.20–0.25, except for the Southwest of the Iberian Peninsula, Southern Italy and Turkey, where values from 0.30 to 0.35 are reached. These would be areas where uncertainties on starting values could lead to the largest erroneous long-term predictions of DSL at these R_0 levels. On the contrary, the spatial distribution for 5.0 and 10.0 mm/day becomes more complex, the South-western Iberian Peninsula, Southern Italy and Turkey still keeping the highest values of λ_1. Considerable values also appear at high latitudes and the spatial heterogeneity increases in Central and Western Europe. Then, whereas the predictive instability of DSL does not generally increase with R_0, its spatial distribution becomes more complex. Additionally, given that the first Lyapunov exponent is positive for all rain gauges and levels R_0, the mechanism governing DSL series has a degree of predictive instability and chaotic behaviour and it could be assumed as dissipative (Kolmogorov entropy different from zero).

Table 2 lists expected values, standard deviations and ranks of variation of the sum of all Lyapunov exponents, S_T, and Kaplan-Yorke dimension, D_{KY}. It can be concluded that slight spatial variation of these parameters exists. Whatever the level R_0, the strange attractors corresponding to every DSL series are characterised by a very similar fractal dimension, close to 13.5 and hardly ever exceeding 14.0. The dissipative and notable chaotic behaviour of the DSL series is confirmed by the average number, $< N_P >$, of positive Lyapunov exponents for the four thresholds R_0, ranging from 6.6 to 6.8, in comparison with the maximum reconstructed dimension ($m = 15$) used to obtain stationary values of the Lyapunov exponents. Both characteristics, as the D_{KY} dimension, depict a low spatial variety, as the maximum range of N_P (5–8) is detected for 0.1 mm/day and the minimum (6–7) for 1.0 mm/day. Then, in spite of the spatial variability of the other parameters of the reconstruction analyses, a common feature of the dynamical system governing European DSLs is a structure of strange attractors with fractal dimensions within a narrow range (12.6–14.1), except for the threshold of 10.0 mm/day, for which strange attractors with dimensions below 11.0 are detected.

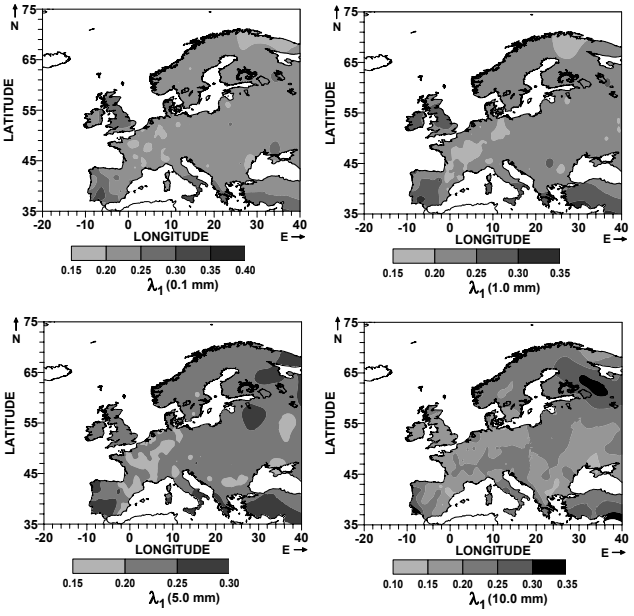

Fig. 11. Spatial distribution of the first positive Lyapunov exponent for thresholds of 0.1, 1.0, 5.0 and 10.0 mm/day.

5 Conclusions

Several concepts of fractal analysis and dynamic system theory applied to 267 European daily rainfall series recorded along 50 years, and distinguishing four different thresholds of daily rainfall, have permitted to estimate the most relevant features regarding randomness, predictability and predictive instability of the DSL regime in Europe. The behaviour of a DSL regime is a very relevant feature taking into account that drought periods (long dry spells or successive dry spells of moderate length) could affect water supplies, agriculture, industry and many other human activities.

Dry spell regimes in Europe are characterised by a notable variety of spatial patterns depending on the threshold R_0. The main features are:

– The lacunarity can be represented by Cantor or random Cantor sets. It is observed that the percentage of lacunarity curves represented by random Cantor sets increases with R_0. In spite of this, a non negligible percentage of DSL series for 10.0 mm/day should be better represented by other models different than Cantor or random Cantor sets.

– Hurst exponents suggest randomness, persistence or anti-persistence, the most complex spatial distribution of H corresponding to 5.0 and 10.0 mm/day. In agreement with the meaning of the Hurst exponent, autoregressive processes would be only applicable to DSL series with clear persistence (H well exceeding 0.5). Although Europe is characterised by Hurst exponents exceeding 0.5, especially for 0.1 and 1.0 mm/day, values of H within the 0.6–0.7 interval are not very common. Consequently, a predictive scheme based on time trends (persistence) would not be very efficient, at least from the point of view of the rescaled analysis.

– The minimum number of nonlinear equations (asymptotic correlation dimension, μ^*) required to describe the physical process governing the DSLs varies from one place to another and with the threshold, and ranges from a relatively simple system of three equations up to a much more complex eight-equation system. An example of this variability is given by comparing the behaviour of μ^* for an area of Western Europe including parts of France, Germany and Belgium. Whereas for 0.1 and 1.0 mm/day the necessary number of nonlinear equations ranges from 7 to 8, it decreases to 5–6 for 5.0 and 10.0 mm/day. A similar decrease of the predictive complexity is detected, for instance, for western Iberian Peninsula.

– Random components disturbing the nonlinear system of equations are notable in all cases taking into account that a high embedding dimension d_E is always necessary to reach stationary values of μ.

– The loss of memory of the dynamic system governing DSL regimes is quantified by the Kolmogorov entropy, κ. The values of κ vary within a wider range for 5.0 and 10.0 mm/day than for the lowest thresholds. This is a relevant fact if a prediction is to be attempted in terms of autoregressive processes, because the number of useful consecutive DSLs for the predictive process diminishes when κ increases.

– The predictive instability is detected for all DSL series and thresholds, with ranges for the first positive Lyapunov exponents (0.15 to 0.40) quite similar for 0.1, 1.0, 5.0 and 10.0 mm/day. Thus, predictive instability is quite similar for all Europe, except for the southwest of the Iberian Peninsula, where Lyapunov exponents reach maxima close to 0.35 whatever the threshold.

– Only the Kaplan-York dimension, D_{KY}, characterising the fractal dimension of the strange attractors governing the successive DSLs, shows a common pattern for all thresholds R_0. This dimension is constrained to a narrow range from a minimum exceeding 12.0 to a maximum close to 14.0 and the number of positive Lyapunov exponents is very similar for all gauges and thresholds. Only for 10.0 mm/day the minimum dimension decreases to 11.0. The high dimension D_{KY} is a clear sign of complexity. To obtain aperiodic stable trajectories around the attractor describing the physical process it is necessary to generate reconstruction vectors z_j of dimension at least 11 or 12.

A single predictive strategy for all rain gauges and thresholds has to be discarded given that all fractal parameters depend on the geographic location and the threshold level. It can be assumed that, at local scale, the effects of atmospheric dynamics governing the rainfall regime (and dry spell regimes) may be influenced by the orography, continental climate or the vicinity to the Atlantic and Artic Oceans and Mediterranean Sea. Thus, lacunarity, rescaled analysis and reconstruction theorem results at local scale should be taken into account to decide the best predictive strategy.

Some strategies could be based on time trends and autoregressive processes for evident persistence (H clearly exceeding 0.5) and low Kolmogorov entropy, guaranteeing small loss of memory of the physical system. These strategies could be termed as statistical predictive methods. Other strategies would be dynamical predictive methods, based on solving nonlinear equation systems describing the physical process, the minimum number of required equations fixed by the correlation dimension. It should be remembered that the success of this predictive process should be strongly based on an accurate determination of starting conditions, due to the predictive instability generated by positive Lyapunov exponents. Finally, if fractal parameters are not appropriate for none of the previous predictive strategies, the generation of

DSL series with the convenient gap size G is a viable alternative when lacunarity is well fitted to Cantor or random Cantor sets.

Acknowledgements. This research was supported by the Ministry of Science and Technology, Spanish Government, project CGL2008-00869/BTE.

Edited by: Z. Toth
Reviewed by: two anonymous referees

References

Burgueño, A., Martínez, M. D., Lana, X., and Serra, C.: Statistical distribution of the daily rainfall regime in Catalonia (NE Spain) for the years 1950–2000, Int. J. Climatol., 25, 1381–1403, 2005.

Cohen, A. and Procaccia, I.: Estimation of Kolmogorov entropy from time signals of dissipative and conservative dynamical systems, Phys. Rev. A, 31, 1872–1882, 1983.

Diks, C.: Nonlinear Time Series Analysis. Methods and Applications, in: Nonlinear Time Series and Chaos (4), World Scientific, London, 209 pp., 1999.

Eckmann, J. P., Oliffson, S., Ruelle, D., and Cilliberto, S.: Lyapunov exponents from time series. Phys. Rev. A, 34(6), 4971–4979, 1986.

Fedder, J.: Fractals, edited by: Plenum, New York USA, 1988.

Goltz, Ch.: Fractal and Chaotic properties of Earthquakes, in: Lecture Notes in Earth Sciences, 77, Springer, Berlin, 175 pp., 1997.

Grassberger, P. and Procaccia I.: Characterization of strange attractors, Phys. Rev. Lett., 50, 346–349, 1983a.

Grassberger, P. and Procaccia, I.: Estimation of the Kolmogorov entropy from a chaotic signal, Phys. Rev. A, 28, p. 2591, 1983b.

Grassberger, P., Schreiber, T., and Shaffrath, C.: Nonlinear time sequence analysis, Int. J. Bifurcat. Chaos, 1, 521–547, 1991.

Harris, D., Menabde, M., Seed, A., and Austin, G.: Multifractal characterization of rain fields with a strong orographic influence, J. Geophys. Res., 101, 26405–26414, 1996.

Hubert, P., Tessier, Y., Lovejoy, S., Shertzer, D., Schmitt, F., Ladoy, P., Carbonnel, J. P., Violette, S., and Desurosne, I.: Multifractal and extreme rainfall events, Geophys. Res. Lett., 20(10), 931–934, 1993.

Kaplan, J. K. and Yorke, J. A.: Chaotic behaviour of multidimensional difference equations, in: Functional Difference Equations and Approximation of Fixed Points, edited by: Walter, H. O. and Peitgen, H. O., Springer Verlag, Berlin, 730, 204–227, 1979.

Klein Tank, A. M. G., Wijngaard, J. B., Können, G. P., Böhm, R., Demarée, G., Gocheva, A., Mileta, M., Pashiardis, S., Hejkrlik, L., Kern-Hansen, C., Heino, R., Bessemoulin, P., Müller-Westermeier, G., Tzanakou, M., Szalai, S., Pálsdóttir, T., Fitzgerald, D., Rubin, S., Capaldo, M., Maugeri, M., Leitass, A., Bukantis, A., Aberfeld, R., Van Engelen, A. F. V., Forland, E., Mietus, M., Coelho, F., Mares, C., Razuvaev, V., Nieplova, E., Cegnar, T., López, J. A. J., Dahlström, B., Moberg, A., Kirchhofer, W., Ceylan, A., Pachaliuk, O., Alexander, L. V., and Petrovic, P.: Daily dataset of 20-th Century surface air temperature and precipitation series for the European climate assessment, Int. J. Climatol., 22, 1441–1453, 2002.

Korvin, G.: Fractals Models in the Earth Sciences, Elsevier, Amsterdam, 396 pp., 1992.

Lana, X., Martínez, M. D., Serra, C., and Burgueño, A.: Spatial and temporal variability of the daily rainfall regime for Catalonia (NE Spain), 1950–2000, Int. J. Climatol., 24, 613–641, 2004.

Lana, X., Martínez, M. D., Posadas, A. M., and Canas, J. A.: Fractal behaviour of the seismicity in the Southern Iberian Peninsula, Nonlin. Processes Geophys., 12, 353–361, doi:10.5194/npg-12-353-2005, 2005.

Lana, X., Martínez, M. D., Burgueño, A., Serra, C., Martín-Vide, J., and Gómez, L.: Distribution of long dry spells in the Iberian Peninsula, years 1951–1990, Int. J. Climatol., 26, 1999–2021, 2006.

Lima, M. I. P. and Grasman, J.: Multifractal analysis of 15-min and daily rainfall from a semi-arid region in Portugal, J. Hydrol., 220, 1–11, 1999.

Lovejoy, S. and Mandelbrot, B. B.: Fractal properties of rain and a fractal model, Tellus A, 37, 209–232, 1985.

Mandelbrot, B. B.: The Fractal Geometry of Nature, Freeman, San Francisco, 1982.

Martínez, M. D., Lana, X., Burgueño, A., and Serra, C.: Lacunarity, predictability and predictive instability of the daily pluviometric regime in the Iberian Peninsula, Nonlin. Processes Geophys., 14, 109–121, doi:10.5194/npg-14-109-2007, 2007a.

Martínez, M. D., Lana, X., Burgueño, A., and Serra, C.: Spatial and temporal daily rainfall regime in Catalonia (NE Spain) derived from four precipitation indices, years 1950–2000, Int. J. Climatol., 27, 123–138, 2007b.

Martínez, M.D., Lana, X., Burgueño, A., and Serra, C.: Predictability of the monthly North Atlantic Oscillation index based on fractal analyses and dynamic system theory, Nonlin. Processes Geophys., 17, 93–101, doi:10.5194/npg-17-93-2010, 2010.

Mazzarella, A.: Multifractal dynamic rainfall process in Italy, Theor. Appl. Climatol., 63, 73–78, 1999.

Mazzarella, A. and Tranfaglia, G.: Fractal characterization of geophysical measuring networks and implications for an optimal location of additional stations: an application to a rain-gauge network, Theor. Appl. Climatol., 65, 157–163, 2000.

Miranda, J. G. V. and Andrade, R. F. S.: Rescaled range analysis of pluviometric records in Northeast Brazil, Theor. Appl. Climatol., 63, 79–88, 1999.

Miranda, J. G. V. and Andrade, R. F. S.: R/S analysis of pluviometric records: comparison with numerical experiments, Physica A, 295, 38–41, 2001.

Miranda, J. G. V., Andrade, R. F. S., da Silva, A. B., Ferreira, C. S., González, A. P., and Carrera López, J. L.: Temporal and spatial persistence in rainfall records from Northeast Brazil and Galicia (Spain), Theor. Appl. Climatol., 77, 113–121, 2004.

Olsson, J., Niemczynowicz, J., and Berndtsson, R.: Fractal analysis of high-resolution rainfall time series, J. Geophys. Res., 98, 23265–23274, 1993.

Oñate, J. J.: Fractal analysis of climatic data: annual precipitation records in Spain, Theor. Appl. Climatol., 56, 83–87, 1997.

Rodríguez-Iturbe, I., Febres de Ower, B., Sharifi, M. B., and Georgakakos, K. P.: Chaos in rainfall, Water Resour. Res., 25, 1667–1675, 1989.

Ruelle, D.: Deterministic chaos. The science and the fiction, Proc. R. Soc. Lon. Ser. A, 427, 241–248, 1990.

Salas, J. D., Kim, H. S., Eykholt, R., Burlando, P., and Green, T. R.: Aggregation and sampling in deterministic chaos: implications for chaos identification in hydrological processes, Nonlin. Processes Geophys., 12, 557–567, doi:10.5194/npg-12-557-2005, 2005.

Sivakumar, B.: Rainfall dynamics at different temporal scales: A chaotic perspective, Hydrol. Earth Syst. Sci., 5, 645–652, doi:10.5194/hess-5-645-2001, 2001a.

Sivakumar, B.: Is a chaotic multifractal approach for rainfall possible?, Hydrol. Process., 15, 943–955, 2001b.

Sivakumar, B., Sorooshian, S., Gupta, H. V., and Gao, X.: A chaotical approach to rainfall disaggregation, Water Resour. Res., 37, 61–72, 2001.

Stoop, F. and Meier, P. F.: Evaluation of Lyapunov exponents and scaling functions from time series, J. Opt. Soc. Am. B, 5, 1037–1045, 1988.

Svensson, C., Olsson, J., and Berndtsson, R.: Multifractal properties of daily rainfall in two different climates, Water Resour. Res., 32, 2463–2472, 1996.

Takens, F.: Detecting strange attractors in turbulence, in: Lecture Note in Mathematics, edited by: Rand, D. A. and Young, L. S., Springer, Berlin, 1981.

Tessier, Y., Lovejoy, S., Hubert, P., Shertzer, D., Pecknold, S.: Multifractal analysis and modelling of rainfall and river flows and scaling causal transfer functions, J. Geophys. Res., 101, 26427–26440, 1996.

Turcotte, D. L.: Fractal and Chaos in Geology and Geophysics, 2nd edn., Cambridge University Press, 398 pp., 1997.

Veneziano, D., Bras, R. L., and Niemann, J. D.: Nonlinearity and self-similarity of rainfall in time and a stochastic model, J. Geophys. Res., 101, 26371–26392, 1996.

Whiting, J. P., Lambert, M. F., and Metcalfe, A. V.: Modelling persistence in annual Australia point rainfall, Hydrol. Earth Syst. Sci., 7, 197–211, doi:10.5194/hess-7-197-2003, 2003.

Wijngaard, J. B., Klein Tank, M. G., and Können, G. P.: Homogeneity of 20th century European daily temperature and precipitation series, Int. J. Climatol., 23, 679–692, 2003.

Wolf, A., Swift, J. B., Swinney, H. L., and Vastano, J. A.: Determining Lyapunov exponents from a time series, Physica D, 16, 285–317, 1985.